



Rutile solubility in albite-H₂O and Na₂Si₃O₇-H₂O at high temperatures and pressures by in-situ synchrotron radiation micro-XRF

Craig E. Manning^{a,*}, Max Wilke^b, Christian Schmidt^b, Jean Cauzid^c

^a Department of Earth and Space Sciences, University of California, Los Angeles, CA 90095-1567, USA

^b GeoForschungsZentrum Potsdam, Telegrafenberg, D-14473 Potsdam, Germany

^c Département Sciences de la Terre, et de l'Univers, G2R, Université Henri Poincaré, 54506 Vandœuvre-lès-Nancy, France

ARTICLE INFO

Article history:

Received 18 October 2007

Received in revised form 4 June 2008

Accepted 5 June 2008

Available online 12 June 2008

Editor: R.W. Carlson

Keywords:

rutile solubility

high-field-strength elements

ti mobility

fluid flow

ABSTRACT

Rutile is an important mineral host for high-field strength elements, so its solubility in geologic fluids at high pressure and temperature plays an important role in the crustal and mantle processes that control the terrestrial cycling of these elements. However, experimental measurements of rutile solubility are in conflict by a factor of more than 100 at most studied conditions. We performed new measurements of rutile solubility in H₂O-albite and H₂O-Na₂Si₃O₇ (NS3) fluids by in-situ synchrotron radiation X-ray fluorescence spectroscopy using modified Bassett-type hydrothermal diamond-anvil cells. Minimum detection limits were 1.9 and 2.3 ppm Ti by weight for the two cells. Three albite-H₂O experiments at starting bulk compositions of 2.7, 6.7 and 10.3 wt.% albite involved spectral acquisition at rutile saturation in the presence of albite crystals, melt, or a single homogeneous fluid phase; after accounting for the additional phases, corrected fluid compositions were 0.6 to 7.5 wt.% dissolved silicate over the run conditions. At ≤ 2.7 wt.% albite, rutile dissolution rate was slow and steady state was not achieved at 600–800 °C; however, at higher dissolved albite contents, constant solubility with time was observed. Rutile solubilities in the presence of a single fluid phase at 700 °C, 0.79 GPa, 5.4 wt.% albite, and at 800 °C, 1.10 GPa, 6.7 wt.% albite, were 37 ± 2 and 156 ± 6 ppm, respectively. These data agree with results acquired using hydrothermal piston-cylinder methods with long run times and suppression of new crystal growth, but not with data derived from visual observation in hydrothermal diamond-anvil cells. This discrepancy is likely due to lack of equilibrium in the latter approach. Two experiments in 10 and 30 wt.% NS3 at 660–800 °C, 0.5 ± 0.1 GPa, show extreme concentration-dependent enhancement of rutile solubility to ~ 4500 ppm. The data indicate a strong positive correlation between rutile solubility and Na/Al. Because (Na+K)/Al is likely to be greater than unity in aqueous fluids at high pressure and temperature due to incongruent dissolution of albite and micas, the increase in rutile solubility along the albite-NS3 join points to the possibility of significant Ti transport by silicate-bearing aqueous fluids in the lower crust and upper mantle.

© 2008 Elsevier B.V. All rights reserved.

1. Introduction

The high-field-strength elements (HFSE) are important tracers of processes affecting magma source regions. For example, subduction-zone magmas commonly display a distinctive depletion in HFSE relative to mid-ocean ridge basalt (e.g., Gill, 1981), which is widely assumed to arise, at least in part, from relatively low solubility of such elements in H₂O at subduction-zone conditions. Models of HFSE geochemistry at these conditions are based chiefly on measurements of the solubility and partitioning behavior of rutile in geologic fluids (e.g., Ayers and Watson, 1993; Brenan et al., 1994; Stalder et al., 1998; Foley et al., 2000), because this mineral is a major host for HFSE. However, there is strong disagreement about rutile solubility in

geologic fluids, and the compositions of model mantle-wedge fluids that have been explored are limited.

Four studies have been conducted on the solubility of rutile in H₂O at high pressure (*P*) and temperature (*T*): Ayers and Watson (1993), Audétat and Keppler (2005), Tropper and Manning (2005) and Antignano and Manning (in press). The results give rutile solubilities in H₂O that differ by more than 100 times at a given *P* and *T*. For example, at 1000 °C, 2 GPa, the results of Ayers and Watson yield Ti concentration in rutile-saturated H₂O of 2273 ppm, whereas values of 146, 109, and 14 ppm are measured or predicted respectively by Tropper and Manning (2005), Antignano and Manning (in press) and Audétat and Keppler (2005). The differences are much greater than the reported uncertainties in the respective studies, give changes with pressure of opposite sign, and persist when components such as NaAlSi₃O₈ (albite) are added. Though such large discrepancies caution that our understanding of the behavior of Ti – and by extension other

* Corresponding author. Tel.: +1 310 206 3290; fax: +1 310 825 2779.
E-mail address: manning@ess.ucla.edu (C.E. Manning).

HFSE – remains poor, it might be concluded that despite large uncertainty, the generally low solubilities at the conditions of interest imply that Ti is largely conserved during subduction-zone metasomatic processes. However, observations of rutile in hydrothermal veins formed in subduction-zone rocks (e.g., Gao and Klemd, 2001; Rubatto and Hermann, 2003; Gao et al., 2007; John et al., 2008) demonstrate that geologic fluids can mobilize significant Ti (cf., Jiang et al., 2005). Thus, independent of the disagreement, it is probable that previous experimental work has not adequately probed the compositional space accessible to high *P* fluids.

In an attempt to resolve conflicts among the previous experimental studies and to expand fluid compositions in which rutile solubility has been measured, we conducted synchrotron radiation X-ray fluorescence (XRF) measurements on rutile-saturated albite–H₂O and Na₂Si₃O₇–H₂O fluids in hydrothermal diamond-anvil cells. The measurements represent the first direct, in-situ determinations of Ti concentration in high *P*–*T* fluids, and provide a basis for evaluating the controls on rutile solubility in fluids of the deep crust and upper mantle.

2. Methods

2.1. Experimental setup

The experiments employed two Bassett-type hydrothermal diamond-anvil cells (HDAC). The cells were modified from the original design of Bassett et al. (1993) to optimize acquisition of synchrotron radiation XRF and X-ray absorption spectra of fluids (Schmidt and Rickers, 2003; Wilke et al., 2006). Each cell had a 60- μ m-deep recess (Fig. 1) in the culet face of one of the anvils. In cell HDAC-A (Wilke et al., 2006), the recess was mechanically drilled and had a maximum diameter of 300 μ m (a conical recess \sim 1.5 mm deep was also drilled in the table face of the same diamond). In cell HDAC-B (Schmidt and Rickers, 2003), the recess was created by focused-ion-beam milling (Wirth, 2004) and had a diameter of 200 μ m. The recesses permit collection of the fluorescence signal at 90° to the incident beam in its polarization plane, such that contributions to the signal from elastic and inelastic scattering by the sampled fluid and cell components (mainly diamond) are minimized, and the fluorescence X-rays that reach the detector are generated almost exclusively in the recess volume. Thus, unwanted contributions to the XRF signal from phases in other portions of the sample chamber can be avoided. The path length of the fluorescence X-rays through the diamonds was about 400 \pm 50 μ m.

The sample chamber of the HDACs consisted of the recess at the culet face and a cylindrical hole in the Re gasket separating the two diamond anvils. The gaskets had an initial thickness of 125 μ m and a hole diameter of 330–510 μ m. At the start of each experiment, a gasket was mounted on the lower anvil. A rutile crystal, silicate glass chip and water were then loaded into the gasket hole. The rutile crystal was placed on the culet face of the anvil lacking a recess, at the edge of the gasket wall. This ensured that fluorescence X-rays generated by excitation of Ti in rutile did not reach the detector. The silicate glass (Na₂Si₃O₇, NS3, or NaAlSi₃O₈, albite) was added as a triangular chip of known thickness, which permitted accurate calculation of glass volume from the chip dimensions. The mass of the glass was calculated from its volume using a density of 2.4 g/cm³ (Mazurin et al., 1983, 1987). The mass of the fluid was obtained from the volume of the sample chamber (the volume of the gasket hole plus that of the recess, as determined by optical micrometry), less the volume of the glass piece. Before the sample chamber was sealed by slight compression of the gasket between the anvils, a small amount of water was allowed to leak out until the volume ratio of the produced air bubble and the remaining liquid indicated that water density upon homogenization would be \sim 0.6–0.7 g/cm³. Care was taken to compress the gasket just enough to seal the sample chamber. This minimized the reduction of chamber volume due to gasket flow

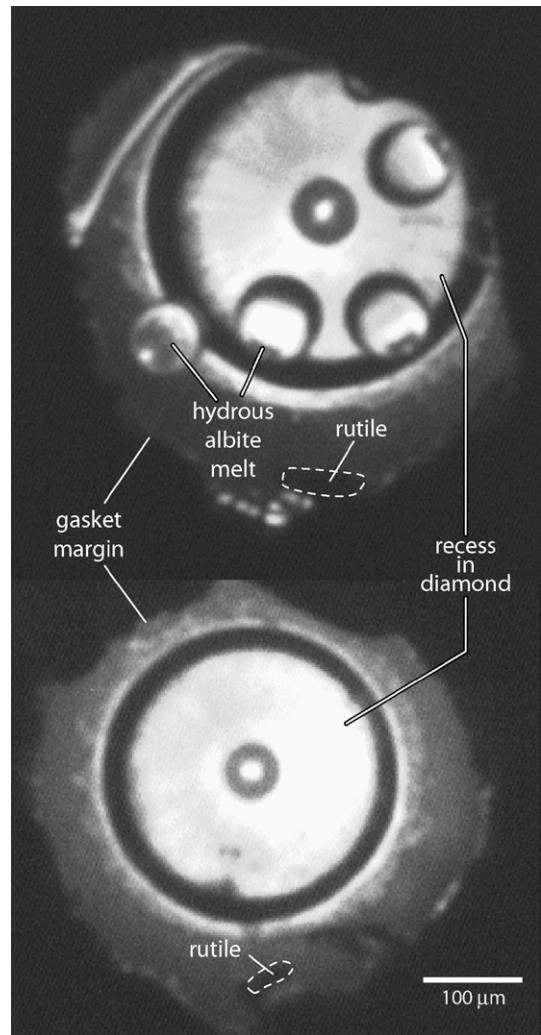


Fig. 1. Photomicrographs of horizontally mounted HDAC, showing sample chambers with recesses. View toward X-ray beam. Upper image shows HDAC A at high *P* and *T*, at conditions of hydrous albite melt + aqueous fluid stability. Rutile crystal is on culet face at base of cell; recess contains fluid + melt. Lower image shows HDAC B at high *P*–*T* where only a single fluid phase is stable.

during heating. Estimated uncertainty in fluid composition from all sources is \pm 1 wt.%.

2.2. Experimental approach

The cells were heated externally by NiCr coils around the tungsten carbide seats that support the anvils. Temperature was measured using K-type thermocouples attached to the diamonds and controlled to within \pm 0.5 °C of the set value using a Eurotherm 2704 controller. The actual temperature in the sample chamber was calibrated based on measurements of the melting point of halite at atmospheric pressure. During heating, oxidation of metallic parts was prevented by flushing the cell with 96% He–4% H₂ gas. Utilization of this gas mixture also reduced absorption of Ti K α fluorescence X-rays along the path towards the detector.

Three to six heating cycles were conducted for each experiment on a particular bulk composition. A typical cycle consisted of heating the cell mounted in a position for optical observation and recording temperatures of phase transitions. After the desired temperature was reached, the cell was rotated around the vertical axis into the position for XRF spectral acquisition and aligned with the beam and the fluorescence detector. After alignment, the Ti K α signal was scanned from the position of the rutile grain towards the center of the recess to

verify that the recorded Ti K α signal was solely from the fluid phase. Typically, two to three consecutive XRF spectra were then recorded at a given temperature. The total time during which the cell was held at each temperature was usually 40–50 min. After spectral acquisition, the cell was cooled and the liquid–vapor homogenization temperature of the aqueous phase was measured. This procedure was then repeated by heating the cell to a higher temperature; the maximum temperature was 800 °C. In several cases, early cycles involved heating to low temperature and cooling, without collection of XRF spectra, chiefly to evaluate gasket behavior and/or integrity. In two cases (Table 1), the cell was not cooled between heating steps because constant homogenization temperature over consecutive cycles had established isochoric behavior.

The pressure at the experimental temperature was calculated from the equation of state of H₂O of Wagner and Pruss (2002) using the density of the aqueous fluid, as determined from its liquid–vapor homogenization temperature measured after spectral acquisition. The volumetric effect of dissolved solids in the system Na₂O–Al₂O₃–SiO₂ is assumed to be negligible. Mysen and Wheeler (2000) found that, at 1000 °C, 0.8–1.0 GPa, the density of silicate-saturated H₂O (1–6 wt.% silicate) is 2–10% greater than that of pure H₂O. Their data indicate that this difference will diminish with decreasing temperature at these pressures. Accordingly, our assumption is probably reasonable for experiments with ≤ 10 wt.% dissolved silicate; however, calculated

pressure in experiment NS3-1, with 30.6 wt.% dissolved silicate, is more uncertain.

2.3. XRF spectroscopy

The experiments were performed at the European Synchrotron Radiation Facility, Grenoble, France, at the micro-focus beamline ID 22. The synchrotron beam was focused to a size of $1.6 \times 5 \mu\text{m}^2$ using Kirkpatrick–Baez mirrors. The excitation energy was set to 10 keV using a Si (111) double-crystal monochromator. This energy was chosen to avoid excitation of Re L fluorescence from the gasket. The XRF spectra were recorded using a 13-element Si(Li) solid-state detector. However, only 4 elements recorded the signal due to the small aperture of the cell. The data analysis showed that the signal from the central detector element, which gave the best signal-to-background ratio, was sufficient to determine the Ti concentrations because adding the signal from the three other elements did not improve the signal-to-background ratio. Spectral acquisition involved initial counting for 100 s, and then one or more counting periods of 1000 s. Net intensities of the fluorescence peaks were determined by fitting the spectra using PyMCA (Solé et al., 2007). Peak intensities were corrected for absorption in the fluid using the fluid composition (silicate component and water) and density. These corrected intensities were normalized to the intensity of the incoming beam.

Table 1
Experimental results

Cycle	Temperature (°C)	Pressure (GPa)	Acquisition time (s)	Elapsed time (min)	Dissolved silicate (wt.%)	Ti (ppm)	Phases	Remarks
<i>Albite-3, HDAC-A, bulk composition: 2.7 wt.% albite</i>								
2	700	1.23	1000	29	2.7	64(5)	F	
2	700	1.23	1000	46	2.7	77(5)	F	
3	752	1.30	1000	19	2.7	107(7)	F	
3	752	1.30	1000	37	2.7	127(7)	F	
5	800	1.19	100	3	2.7	152(15)	F	
5	800	1.19	1000	21	2.7	156(9)	F	
5	800	1.19	1000	39	2.7	183(10)	F	
<i>Albite-2, HDAC-A, bulk composition: 6.7 wt.% albite</i>								
2	700	0.79	100	6	5.4*	31(6)	XF	
2	700	0.79	1000	24	5.4*	37(3)	XF	
2	700	0.79	1000	42	5.4*	37(3)	XF	
3	700	0.79	100	24	5.4*	32(6)	XF	Cell reheated to 700 °C
3	700	0.79	1000	42	5.4*	39(3)	XF	
3	800	1.11	100	15	6.7	153(17)	F	Heated from 700 °C
3	800	1.11	1000	34	6.7	145(9)	F	
3	800	1.11	1000	52	6.7	168(9)	F	
<i>Albite-1, HDAC-A, bulk composition: 10.3 wt.% albite</i>								
4	600	0.31	1000	22	0.6*	4(1)	XF	Heated from 500 °C
4	600	0.31	1000	39	0.6*	6(1)	XF	
5	700	0.44	1000	20	1.6*	19(2)	XF	
6	800	0.71	100	4	7.5*	185(17)	MF	X→M at 762 °C
6	800	0.71	1000	23	7.5*	185(10)	MF	
<i>NS3-2, HDAC-B, bulk composition: 9.3 wt.% NS3</i>								
3	660	0.34	1000	27	9.3	214(15)	F	Qz supersaturated
4	730	0.44	100	11	9.3	251(25)	F	Qz supersaturated
4	730	0.44	1000	29	9.3	286(20)	F	Qz supersaturated
5	800	0.59	100	2	9.3	406(37)	F	
5	800	0.59	1000	20	9.3	410(28)	F	
<i>NS3-1, HDAC-B, bulk composition: 30.6 wt.% NS3</i>								
1	660	0.36	1000	40	30.6	4490(272)	F	Qz supersaturated
2	730	0.49	100	22	30.6	4019(277)	F	Qz supersaturated
2	730	0.49	1000	40	30.6	3986(242)	F	Qz supersaturated
3	800	0.62	100	13	30.6	4266(298)	F	Qz supersaturated
3	800	0.62	1000	31	30.6	4410(268)	F	Qz supersaturated

Explanation: Bulk composition determined from mass H₂O and silicate glass at start of each experiment; actual fluid composition at high *P–T* changed with phases present. Elapsed time is the time at end of spectral acquisition less the time at which heating to the experimental temperature was completed. Abbreviations: X: albite crystals; F: aqueous fluid; M: silicate melt. Asterisk indicates dissolved silicate calculated by polynomial fits, to experimentally determined albite solubility in H₂O (Anderson and Burnham, 1983); estimated error is ± 1 wt.%. Dissolved silicate in melt-saturated H₂O approximated using the same equations, but estimated error is larger (± 2 wt.%). Parenthetical numbers denote 1σ errors in last significant digits.

Intensities were calibrated by measurements of a standard solution (1005 mg Ti/L solution; matrix: H₂O+5 vol.% HNO₃) that were loaded into the sample chamber of the cell. The actual Ti concentration of the solution after loading was corrected for minor evaporative loss of matrix solution by measurement of the ice melting temperature in the presence of vapor (Schmidt et al., 2006, Schmidt et al., 2007). The uncertainties in the actual Ti concentration of the standard solutions were 3% (HDAC-A) and 5% (HDAC-B).

The sensitivity of the experimental setup was evaluated using spectra collected from both cells when empty and when containing the standard solution (Fig. 2). All peaks other than Ti are due to excitation by scattered radiation from parts of the cell or other materials in proximity to the X-ray beam. The empty-cell spectrum indicates that this scattered background does not contribute to the Ti signal. Estimation of absolute sensitivity (i.e., signal per mass unit) requires knowledge of the excitation volume and the excited mass. We estimated the effective excitation volume to be $\sim 4.5 \times 10^{-10} \text{ cm}^3$, based on the depth of the recess and the focal size of the beam. Absolute sensitivities normalized to the photon flux were 1.82×10^{-11} and 2.28×10^{-11} cts/s/pg/photon for HDAC A and HDAC B, respectively; relative sensitivities normalized to the photon flux were 8.17×10^{-15} (A) and 1.03×10^{-14} cts/s/ppm/photon (B). The absolute and relative values indicate a 25% difference between the two cells. The fact that the size of excited volume need not be known for the relative sensitivity shows that the excitation volumes of the two cells must be similar, regardless of the exact size of this volume. Otherwise absolute and relative sensitivities would differ under the given assumptions.

The minimum detection limit (mdl) was calculated from $\text{mdl} = 3c\sqrt{B/I}$ (e.g. Haller and Knöchel, 1996), where c is the concentration, B the background intensity and I the peak intensity. The mdl values determined from standard-solution spectra were 1.9 ppm for HDAC-A and 2.3 ppm for HDAC-B. The standard deviation provided in Table 1 is propagated from the uncertainty in the Ti intensity from the fits of the spectra and the uncertainty of the concentrations in the standard solutions.

2.4. Fluid composition

The NS3 glass dissolved completely in H₂O to produce one fluid at all experimental conditions, but albite glass did so only at the lowest

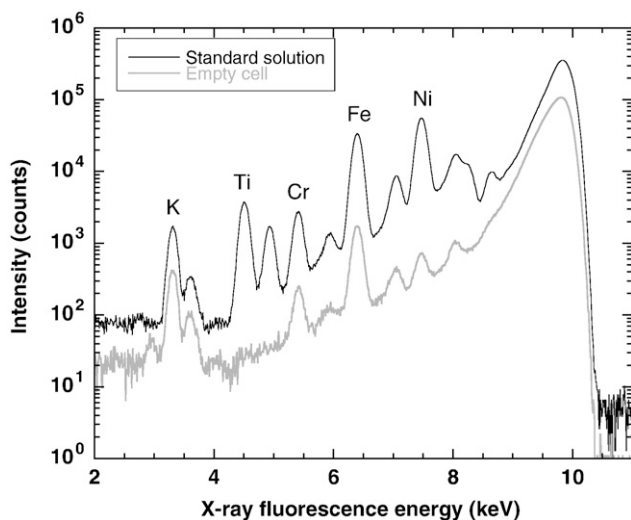


Fig. 2. X-ray fluorescence spectra of empty cell (lower) and cell filled with standard solution (upper). The standard solution contained 993 ppm Ti, based on correction for evaporation after loading of standard solution with 1005 ppm Ti. Comparison of the two spectra shows negligible Ti background in the empty cell. All other peaks are due to excitation by scattered radiation of the diamond cell and other materials in the vicinity of the beam path.

concentrations or the highest P and T . Where an additional phase was present (albite crystals or melt), fluid composition was calculated from polynomial fits to the isothermal variation in albite solubility with P (Anderson and Burnham, 1983). The investigated conditions were generally within the range of the data of Anderson and Burnham (1983) or required only minor extrapolation; fluid compositions so determined were assumed to be accurate to ± 1 wt.%. However, at the highest P , T and albite concentration investigated (Table 1), melt was present instead of albite crystals. In this case, melt solubility was assumed to be the same as albite solubility, as predicted by extrapolation of the Anderson and Burnham (1983) data to 800 °C, but was assigned a larger uncertainty of ± 2 wt.%. All Ti concentrations are reported as mg per kg solution (ppm).

3. Results and discussion

We determined Ti concentrations in the presence of rutile at high P and T for three albite-H₂O bulk compositions and two NS3-H₂O bulk compositions. Results are given in Table 1 and Fig. 3.

3.1. Phases present

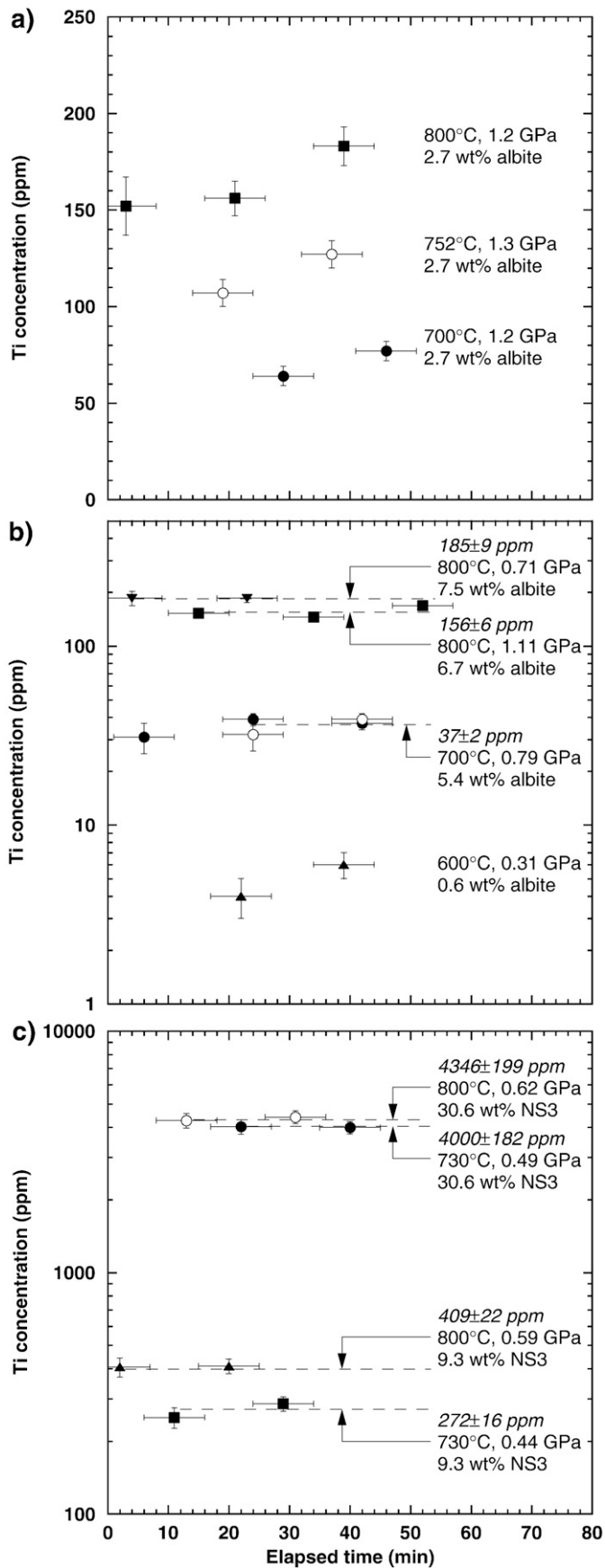
Depending on bulk composition, phases present with rutile at the P - T of spectral acquisition were fluid+crystals, fluid+melt (Fig. 1a) or a single fluid phase (Fig. 1b). In the albite-H₂O experiments, the crystals were assumed to be albite, based on the observed transitions from crystals to melt (Albite-1) and to a single fluid (Albite-2) at 700–800 °C at 0.8–1.1 GPa (Table 1), which are similar to conditions determined independently (e.g., Stalder et al., 2000). Previous work has shown that albite dissolves incongruently at high P and T (Currie, 1968; Anderson and Burnham, 1983; Stalder et al., 2000; Shmulovich et al., 2001); however, no other residual minerals were observed. We infer that experiment durations were shorter than required for nucleation of any residual phases.

The NS3-H₂O experiments were supersaturated with respect to quartz at some conditions (Table 1). In NS3-2, quartz formed upon heating during cycle 5. These crystals dissolved at 757 °C. After cycle 3 of experiment NS3-1, crystals formed at about 500 °C upon reheating and did not completely dissolve during further heating. These crystals were identified as quartz by Raman spectroscopy after the experiments. The formation of quartz in the cell after significant time at elevated T is consistent with a modest nucleation barrier for this phase. Experiments were terminated whenever quartz was observed in the cell.

3.2. Reproducibility and equilibrium

We evaluated reproducibility in experiment Albite-2 (Table 1) by collecting spectra at 700 °C, cooling, then reheating to 700 °C and collecting additional spectra. The two analysis cycles gave the same concentration within 1σ (Table 1, Fig. 3b).

Variations in counting time allowed us to assess the approach to equilibrium in the experiments. Based on time-resolved XRF analyses of fluid during monazite and zircon dissolution experiments in acidic solutions (Schmidt et al., 2006, Schmidt et al., 2007) and previous study of rutile solubility in HDACs (Audéat and Keppler, 2005), we expected that the equilibration time would be of the order of several minutes. However, the data suggest that in the albite-H₂O experiments, there were concentration-dependent variations in equilibration time (Fig. 3). This was established by estimating the elapsed time after an experiment had been brought to a particular temperature from the log files, which was possible to within ± 5 min. At the lowest T , P and dissolved silicate (600 °C, 0.31 GPa, 0.6 wt.% albite), measured Ti concentration after 39 min is higher than that after 22 min by $\sim 2\sigma$. An increase in Ti concentration with time was observed during all cycles and times in experiment Albite-3 (2.7 wt.% albite; Fig. 3a). At 5.4 wt.% albite (Albite-2), Ti concentration after 6 min at 700 °C is



lower than at longer elapsed times, but by less than 1σ . Finally, at 6.7 and 7.5 wt.% albite, Ti concentration was constant at ≥ 6 min (Fig. 3b). Both NS3-H₂O experiments yielded constant solubility with time (Fig. 3c). It is possible that the behavior of experiment Albite-3 was caused by change in the excitation volume in the recess of HDAC-A due to a slow change in position when the cell holder was not thermally equilibrated; however, this is unlikely because the behavior was not observed in all experiments. Instead, it appears that the time required for equilibration in albite solutions is at least several minutes in all cases, and significantly longer (more than several tens of minutes) at low dissolved albite content. Fig. 3 shows weighted mean Ti concentrations for those experiments interpreted to have reached equilibrium.

3.3. Rutile solubility in albite-bearing H₂O

The equilibrium data indicate that Ti solubility at rutile saturation is 37 ± 2 ppm at 700 °C, 0.79 GPa and 5.4 wt.% dissolved albite. Higher solubility of 155 ± 6 ppm was obtained at 800 °C, 1.11 GPa and 6.7 wt.% albite. A general increase in solubility with T , P and/or dissolved albite concentration is consistent with previous findings (Audéat and Keppler, 2005; Antignano and Manning (in press)); however, prior experimental studies yield quite different absolute rutile solubilities in H₂O and albite-H₂O at high P and T . Our results provide additional, independent constraints on this system.

The previous experimental studies on rutile solubility in aqueous solutions at high P and T have employed contrasting approaches. Using hydrothermal piston-cylinder weight-loss techniques (Manning, 1994; Manning and Boettcher, 1994), Tropper and Manning (2005) and Antignano and Manning (in press) measured rutile solubility in H₂O at 700–1150 °C, 0.7–2.0 GPa and obtained much lower values than Ayers and Watson (1993), who used similar methods. Tropper and Manning (2005) attributed the differences to misinterpretation of recrystallized rutile as quench in the experiments of Ayers and Watson (1993). Audéat and Keppler (2005) used visual observation of rutile growth and dissolution in the HDAC and found rutile solubilities in H₂O lower than Tropper and Manning (2005) and Antignano and Manning (in press) by nearly 10 times. A similar discrepancy exists for albite-H₂O solutions. Antignano and Manning (in press) determined rutile solubility in albite-H₂O at 0.7–2.0 GPa, 700–900 °C, and also derived solubilities that were higher than those of Audéat and Keppler (2005) at similar fluid compositions by up to 100 times. Although the stoichiometry of dissolved silicate differed (Antignano and Manning, in press noted incongruent albite dissolution, but Audéat and Keppler, 2005 did not), the disparity was no more than 15% and unlikely to explain the disagreement. The large discrepancies have led to the suggestion that hydrothermal piston-cylinder experiments using weight-loss techniques are unreliable because of difficulty in accounting for new growth of the phase of interest (Audéat and Keppler, 2005).

We collected spectra at two separate conditions where rutile coexisted with only an albite-bearing aqueous phase. These measurements are compared with those of Audéat and Keppler (2005) and Antignano and Manning (in press) at 700 and 800 °C in Fig. 4. Both previous studies indicate an increase in rutile solubility with increasing albite concentration at high P and T . At 700 °C, our measured rutile solubility at 0.79 GPa is within error of the 1 GPa data of Antignano and Manning (in press) (Fig. 4a). Antignano and Manning

Fig. 3. Ti concentration in rutile-saturated fluids as a function of elapsed time at the measurement P - T condition. Elapsed time is the time between attainment of experimental temperature and completion of counting; uncertainty is ± 5 min (see text). Symbols keyed to experimental P , T and fluid composition listed at right; open and filled symbols for the same conditions denote different cycles (Table 1). Errors in Ti concentration are 1σ . Horizontal dashed lines show mean Ti concentrations in those experiments interpreted to have attained equilibrium, weighted by $1/\sigma^2$; values given at right with experimental conditions (see text).

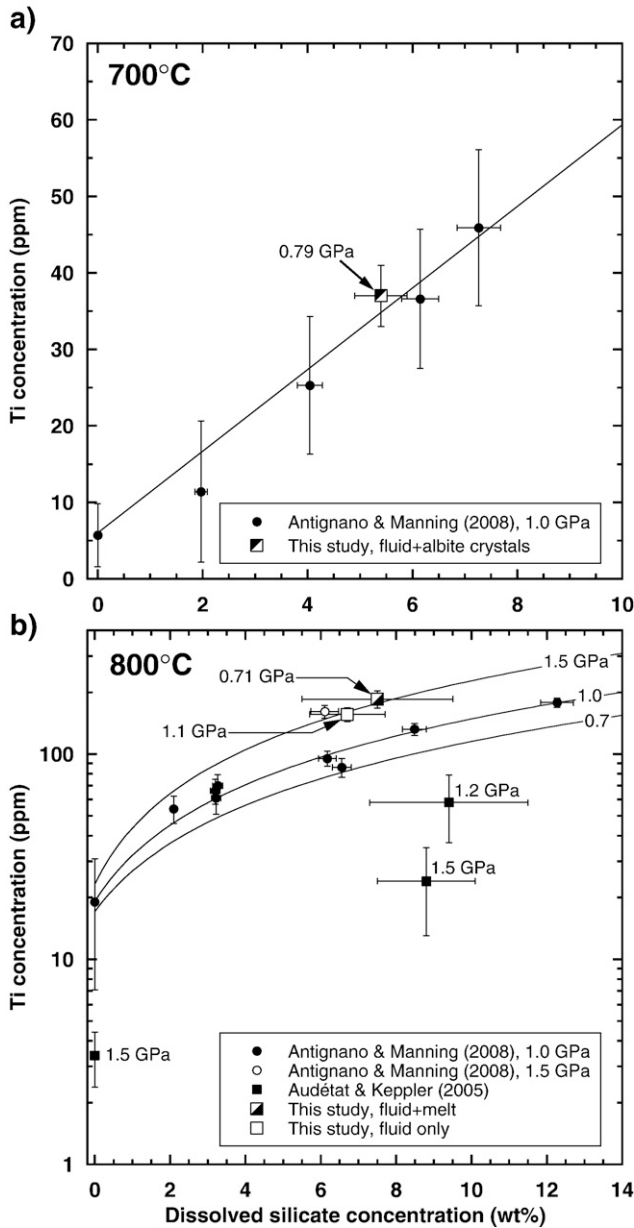


Fig. 4. Ti concentrations vs. dissolved silicate concentration at 700 °C (A) and 800 °C (B); all errors 2σ . In (A), datum from the present study is compared to results of Antignano and Manning (in press) at 1.0 GPa (data, filled circles; fit equation, solid lines). In (B), data from this study are compared to Antignano and Manning (in press) data (1.0 GPa, filled circles, pure-H₂O datum is weighted mean of 3 experiments; 1.5 GPa, open circle) and fit equations (solid lines), as well as to results of Audéat and Keppler (2005; filled squares; pure H₂O datum is calculated from their fit equation and uncertainty is assumed to be 30% relative, based on data in their Table 1). “Dissolved silicate” in this study and Audéat and Keppler (2005) is albite; however Antignano and Manning (in press) observed incongruent dissolution of albite to paragonite/corundum+fluid, so their fluid compositions differ slightly from the other studies. The error bars on their data show the range in dissolved silicate concentration from a maximum for albite stoichiometry (i.e., negligible mass of residual phases) to a minimum derived from fits to the variation in concentration at 600 °C with increasing P (Antignano and Manning, in press).

(in press) found that, at fixed T and albite content, rutile solubility increases slightly with pressure; however, at 700 °C, ≤ 1 GPa, the effect is predicted to be smaller than the uncertainty in the 1 GPa data.

Fig. 4b compares results on rutile solubility in albite-H₂O at 800 °C and a range of P . The data of Antignano and Manning (in press) at 1.0 and 1.5 GPa suggest increasing solubility with P . Our measurement at 1.1 GPa lies between the 1.0 and 1.5 GPa isopleths of Antignano and Manning (in press), although closer to the 1.5 GPa datum. However, we

obtained a Ti concentration that is significantly higher than that inferred by Audéat and Keppler (2005) at similar P (Fig. 4b). The explanation for this difference is most likely the surprisingly slow reaction rates of rutile dissolution, as indicated by the present study. Audéat and Keppler determined solubility by visually monitoring the appearance and disappearance of rutile crystals in an HDAC using heating rates of tens of degrees per minute. If reaction rates are slow, this method will lead to overstepping of the temperature at which complete dissolution would occur had the cell been held at a lower T for longer time. The result would be low apparent solubility, as observed when comparing the results of Audéat and Keppler (2005) to studies involving equilibration times of tens of minutes (this study) to hours (Antignano and Manning, in press).

3.4. Rutile solubility in albite-bearing H₂O saturated with hydrous melt

Our third measurement of rutile solubility in albite-H₂O in which equilibrium can be inferred was at 800 °C, 0.71 GPa, in the presence of hydrous albite melt and fluid with ~ 7.5 wt.% albite. Rutile solubility was 185 ± 9 ppm Ti. In this case, our Ti concentration is significantly higher than that which would be predicted from Audéat and Keppler (2005) or Antignano and Manning (in press). It is also higher than would be predicted from experiment Albite-2 if rutile solubility increases with P as proposed by Antignano and Manning (in press). In light of the generally good agreement between our results and those of Antignano and Manning (in press) in the presence of a single fluid phase, we infer that the presence of melt led to anomalously high Ti concentrations. Hydrous albite melt partitions Ti strongly relative to the fluid phase (Hayden and Watson, 2007; Antignano and Manning, in press). We suggest that excess Ti was measured due to fluorescence of Ti in melt blebs in the sample chamber (Fig. 1a).

3.5. Rutile solubility in NS3-H₂O

Fig. 5 shows the variation in rutile solubility with NS3 content in NS3-H₂O fluid at 660–800 °C, 0.5 ± 0.1 GPa, to >30 wt.% NS3. The fluid is everywhere in the one-phase field, though the system was metastable with respect to quartz at some conditions (Table 1).

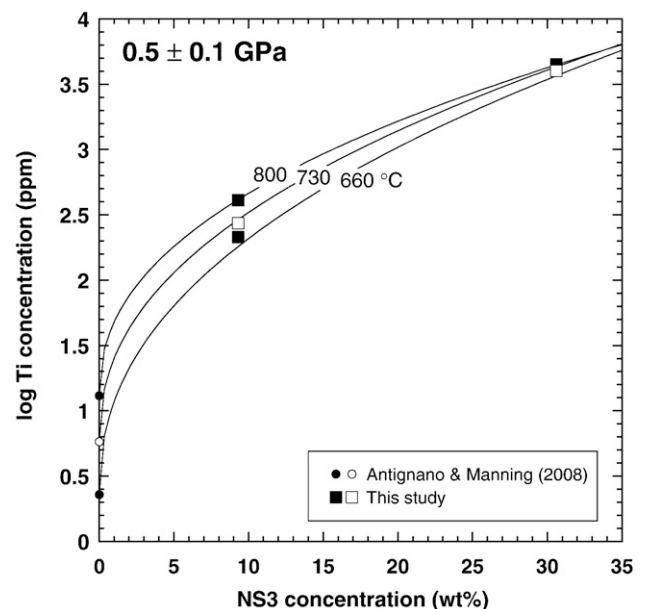


Fig. 5. Ti concentration vs. dissolved Na₂Si₃O₇ concentration at 660 to 800 °C at 0.5 ± 0.1 GPa. 2σ uncertainties are smaller than symbol sizes. Pure H₂O values calculated from Eq. (2) of Antignano and Manning (in press). Solid lines calculated from Eq. (1).

Assuming that there is negligible dependence on P over this small interval, the results indicate that Ti concentration rises with T at constant fluid composition. The T dependence of solubility in pure H_2O is strong (Antignano and Manning, in press); however, this dependence appears to diminish with increasing NS3, such that at 30.6 wt.% NS3, Ti concentrations are nearly identical within the uncertainties in the investigated T range. These features are reproduced by the following fit equation:

$$\log c_{Ti} = \log c_{Ti}^0 + \left(1.71 - 1.07 \times 10^{-3}T\right) c_{NS3}^{0.44} \quad (1)$$

where T is in K, c_{NS3} is NS3 concentration in wt.%, c_{Ti} is Ti concentration in ppm, and c_{Ti}^0 is Ti concentration in pure H_2O in equilibrium with rutile (also in ppm), as calculated from:

$$\log c_{Ti}^0 = 6.173 - 5425/T + 178.4P/T \quad (2)$$

(Antignano and Manning, in press), where T is again in K and P is in GPa. The increase in rutile solubility with NS3 content is strongly nonlinear, such that very high solubilities – up to 0.4 wt.% Ti – are indicated for in these peralkaline solutions.

4. Implications for high P – T fluids

The present results can be used to place preliminary constraints on the nature of Ti dissolution mechanisms at high P and T . As shown in Fig. 4, dissolved albite enhances rutile solubility at a given P and T (Audétat and Keppler, 2005; Antignano and Manning, in press). Rutile solubility is also enhanced by NS3 (Fig. 5). The degree of enhancement can be compared at 700 °C, 0.8 GPa, where dissolved Ti concentration in pure H_2O is 18 ppm (Antignano and Manning, in press). Addition of 5.4 wt.% albite increases solubility to 37 ± 2 ppm; however, a similar concentration of NS3 would have a Ti concentration of 250 ppm (Eq. (1)). Thus, on an equivalent-weight basis, NS3 yields nearly ten times greater enhancement of rutile solubility.

The observation that rutile solubility is higher in Al-free Na-silicate-bearing fluid than in albite-bearing fluid is similar to results on rutile solubility in silicate melts. Dickenson and Hess (1985) found that rutile solubility in K_2O – Al_2O_3 – SiO_2 melts increased isothermally and isobarically with increasing K_2O/Al_2O_3 . For more complex natural magmas, Ryerson and Watson (1987) used the compositional parameter $FM = [Na + K + 2(Ca + Fe + Mg)]Al^{-1}Si^{-1}$ to examine the role of melt composition on rutile solubility. Their results indicate that at constant concentrations of Si and divalent cations, rutile solubility increases with increasing FM, which corresponds to increasing $(Na + K)/Al$. Similar results were obtained by Hayden and Watson (2007) on hydrous melts. The increase in Ti solubility with increasing $(Na + K)/Al$ is consistent with the low melting temperatures in the Na_2O – TiO_2 – SiO_2 system (Hamilton and Cleek, 1958; Glasser and Marr, 1979). These observations suggest formation of alkali-titanate complexes in the melt (Dickenson and Hess, 1985).

The results of the present study suggest that, as in silicate melts, Na–Ti complexing may be important in controlling rutile solubility in high P – T fluids. Na–Al silicates dissolved in H_2O at these conditions form a wide range of solute complexes, but a significant fraction of these complexes are polymerized Al–Si species with one or more bridging oxygens and charge-balancing Na (Manning, 2004, 2007). If this is correct, then Al-free solutions are likely to be less polymerized. The strong inverse correlation between aqueous Al and Ti concentrations suggests that greater dissolved Ti may be accommodated by liberation of Na as Al–Si polymer concentrations decrease.

An increase in Ti concentration with increasing Na/Al is significant because fluids in equilibrium with albite have Na/Al > 1 due to incongruent dissolution of albite (e.g., Anderson and Burnham, 1983; Stalder et al., 2000). Moreover, this ratio increases with increasing P (Anderson and Burnham, 1983; Antignano, 2008). Thus,

the expected increase in rutile solubility with rising P will be compounded by increasing peralkalinity of the fluid phase. As a result, high dissolved Ti concentrations are to be expected in Al-poor environments metasomatized by fluids derived from Na–Al-silicate-bearing lithologies, such as the mantle wedge above subducting oceanic slabs. It has been hypothesized that low-silica, Ti-rich adakites are melts of the mantle wedge that has been metasomatically enriched in Ti and other HFSE by felsic melts derived from the subducting slab (e.g., Martin et al., 2005). The results of the present study suggest that the mobility of Ti, and by analogy other HFSE, may be sufficiently high in appropriate fluid compositions that slab melting need not be invoked to explain HFSE-enriched subduction-zone magmas.

5. Conclusions

- (1) The measurements of standard solutions and of albite– H_2O and NS3– H_2O fluids at rutile saturation at high P and T indicate excellent sensitivity and reproducibility for the analysis of Ti by synchrotron radiation XRF in hydrothermal diamond-anvil cells. Precisions of ~5–10% relative (1σ) at low Ti concentration are a significant improvement over other methods where precision may be no better than 50% relative (Audétat and Keppler, 2005; Tropper and Manning, 2005; Antignano and Manning, in press). In addition, our methods permit the approach to equilibrium to be monitored directly by collection of multiple spectra over time. The minimum detection limit of <3 ppm suggests that the techniques described in this paper offer excellent prospects for evaluation of rutile solubility and dissolution kinetics at relatively low P and T , where Ti concentrations are expected to be quite low.
- (2) The solubility of rutile in albite– H_2O fluids increases with P , T and dissolved albite content. Our results agree well with those of Antignano and Manning (in press), but not with those of Audétat and Keppler (2005). We infer that the rate of the rutile dissolution reaction is unexpectedly slow, which led to overstepping of the dissolution equilibrium and underestimation of rutile solubility in the latter study. Our data indicate that hydrothermal piston-cylinder and HDAC approaches to the determination of mineral solubility can be reconciled.
- (3) The solubility of rutile in NS3– H_2O fluids exhibits a strong positive correlation with dissolved silicate. Peralkaline fluids can be expected to transport significant Ti in lower crustal and mantle environments.
- (4) The increase in rutile solubility with increasing Na/Al points to a Ti dissolution mechanism involving Na–Ti complexing, as in silicate melts.
- (5) The high Ti concentrations in fluids with Na/Al > 1 is important because it is likely that such ratios characterize fluids metasomatizing the mantle wedge. The ability of this type of fluid to transport Ti suggests an alternative mechanism for HFSE enrichment in the source of low-silica adakites.

Acknowledgments

We thank H.J. Reichmann for assistance with the measurements. The manuscript was improved by comments on an early draft by R. Newton, a journal review by J. Brenan, and editorial handling by R. Carlson. The research was funded through support from the ESRF, U.S. National Science Foundation grants EAR-0337170 and 0711521, and the German Academic Exchange Service (DAAD).

References

- Anderson, G.M., Burnham, C.W., 1983. Feldspar solubility and the transport of aluminum under metamorphic conditions. *Am. J. Sci.* 283-A, 283–297.

- Antignano, A., 2008. Apatite and rutile solubility in water-sodium chloride and silicate-bearing fluids at high temperatures and pressures: implications for metamorphic fluids. Unpublished Ph.D. thesis, University of California, Los Angeles, 94 pp.
- Antignano, A., Manning, C.E., 2005. Rutile solubility in H₂O and H₂O-albite at 700–1000 °C and 0.7–2.0 GPa: implications for the aqueous transport of high-field-strength elements at high pressure and temperature. *Chem. Geol.*, in press.
- Audétat, A., Keppler, H., 2005. Solubility of rutile in subduction zone fluids, as determined by experiments in the hydrothermal diamond anvil cell. *Earth Planet. Sci. Lett.* 232, 393–402.
- Ayers, J.C., Watson, E.B., 1993. Rutile solubility and mobility in supercritical aqueous fluids. *Contrib. Mineral. Petrol.* 114, 321–330.
- Bassett, W.A., Shen, A.H., Bucknum, M., Chou, I.-M., 1993. A new diamond anvil cell for hydrothermal studies to 2.5 GPa and from –190 to 1200 °C. *Rev. Sci. Instrum.* 64, 2340–2345.
- Brenan, J.M., Shaw, H.F., Phinney, D.L., Ryerson, F.J., 1994. Rutile-aqueous fluid partitioning of Nb, Ta, Hf, Zr, U and Th: implications for high field strength element depletions in island-arc basalts. *Earth Planet. Sci. Lett.* 128, 327–339.
- Currie, K.L., 1968. On the solubility of albite in supercritical water in the range 400 to 600 °C and 750 to 3500 bars. *Am. J. Sci.* 266, 321–341.
- Dickenson Jr., J.E., Hess, P.C., 1985. Rutile solubility and titanium coordination in silicate melts. *Geochim. Cosmochim. Acta* 49, 2289–2296.
- Foley, S.F., Barth, M.G., Jenner, G.A., 2000. Rutile/melt partition coefficients for trace elements and an assessment of the influence of rutile on the trace element characteristics of subduction zone magmas. *Geochim. Cosmochim. Acta* 64, 933–938.
- Gao, J., Klemd, R., 2001. Primary fluids entrapped at blueschist to eclogite transition: evidence from the Tianshan meta-subduction complex in northwestern China. *Contrib. Mineral. Petrol.* 142, 1–14.
- Gao, J., John, T., Klemd, R., Xiong, X.M., 2007. Mobilization of Ti–Nb–Ta during subduction: evidence from rutile-bearing dehydration segregations and veins hosted in eclogite, Tianshan, NW China. *Geochim. Cosmochim. Acta* 71, 4974–4996.
- Gill, J.B., 1981. *Orogenic Andesites and Plate Tectonics*. Springer-Verlag, Berlin.
- Glasser, F.P., Marr, J., 1979. Phase relations in the system Na₂O–TiO₂–SiO₂. *J. Am. Ceram. Soc.* 62, 42–47.
- Haller, M., Knöchel, A., 1996. X-ray fluorescence analysis using synchrotron radiation (SYXRF). *J. Trace Microprobe Tech.* 14, 461–488.
- Hamilton, E.H., Cleek, G.W., 1958. Properties of sodium titanium silicate glasses. *J. Res. Natl. Bur. Stand.* 61, 89–94.
- Hayden, L.A., Watson, E.B., 2007. Rutile saturation in hydrous siliceous melts and its bearing on Ti-thermometry of quartz and zircon. *Earth Planet. Sci. Lett.* 258, 561–568.
- Jiang, S.Y., Wang, R.C., Xu, X.S., Zhao, K.D., 2005. Mobility of high field strength elements (HFSE) in magmatic-, metamorphic-, and submarine-hydrothermal systems. *Phys. Chem. Earth* 30, 1020–1029.
- John, T., Klemd, R., Gao, J., Garbe-Schönberg, C.-D., 2008. Trace-element mobilization in slabs due to non steady-state fluid-rock interaction: constraints from an eclogite-facies transport vein in blueschist (Tianshan, China). *Lithos* 103, 1–24.
- Manning, C.E., 1994. The solubility of quartz in H₂O in the lower crust and upper mantle. *Geochim. Cosmochim. Acta* 58, 4831–4839.
- Manning, C.E., 2004. The chemistry of subduction-zone fluids. *Earth Planet. Sci. Lett.* 223, 1–16.
- Manning, C.E., 2007. Solubility of corundum + kyanite in H₂O at 700 °C and 10 kbar: evidence for Al–Si complexing at high pressure and temperature. *Geofluids* 7, 258–269.
- Manning, C.E., Boettcher, S.L., 1994. Rapid-quench hydrothermal experiments at mantle pressures and temperatures. *Am. Mineral.* 79, 1153–1158.
- Martin, H., Smithies, R.H., Rapp, R., Moyena, J.-F., Champion, D., 2005. An overview of adakite, tonalite-trondhjemite-granodiorite (TTG), and sanukitoid: relationships and some implications for crustal evolution. *Lithos* 79, 1–24.
- Mazurin, O.V., Streltsina, M.V., Shviko-Shvikovskaya, T.P., 1983. *Handbook of Glass Data, Part A. Silica Glass and Binary Silicate Glasses*. Elsevier, Amsterdam.
- Mazurin, O.V., Streltsina, M.V., Shviko-Shvikovskaya, T.P., 1987. *Handbook of Glass Data, Part C. Ternary Silicate Glasses*. Elsevier, Amsterdam.
- Mysen, B.O., Wheeler, K., 2000. Alkali aluminosilicate-saturated fluids in the earth's upper mantle. *Geochim. Cosmochim. Acta* 64, 4243–4256.
- Rubatto, D., Hermann, J., 2003. Zircon formation during fluid circulation in eclogites (Monviso, Western Alps): implications for Zr and Hf budget in subduction zones. *Geochim. Cosmochim. Acta* 67, 2173–2187.
- Ryerson, F.J., Watson, E.B., 1987. Rutile saturation in magmas: implications for Ti–Nb–Ta depletion in island-arc basalts. *Earth Planet. Sci. Lett.* 86, 225–239.
- Schmidt, C., Rickers, K., 2003. In-situ determination of mineral solubilities in fluids using a hydrothermal diamond-anvil cell and SR-XRF: solubility of AgCl in water. *Am. Mineral.* 88, 288–292.
- Schmidt, C., Rickers, K., Wirth, R., Nasdala, L., Hanchar, J.M., 2006. Low-temperature Zr mobility: Sn in situ synchrotron-radiation XRF study of the effect of radiation damage in zircon on the element release in H₂O+HCl±SiO₂ fluids. *Am. Mineral.* 91, 1211–1215.
- Schmidt, C., Rickers, K., Bilderback, D.H., Huang, R., 2007. In situ synchrotron-radiation XRF study of REE phosphate dissolution in aqueous fluids to 800 °C. *Lithos* 95, 87–102.
- Shmulovich, K.I., Graham, C., Yardley, B., 2001. Quartz, albite and diopside solubilities in H₂O–NaCl and H₂O–CO₂ fluids at 0.5–0.9 GPa. *Contrib. Mineral. Petrol.* 141, 95–108.
- Solé, V.A., Papillon, E., Cotte, M., Walter, P., Susini, J., 2007. A multiplatform code for the analysis of energy-dispersive X-ray fluorescence spectra. *Spectrochim. Acta B* 62, 63–68.
- Stalder, R., Foley, S.F., Brey, G.P., Horn, I., 1998. Mineral-aqueous fluid partitioning of trace elements at 900–1200 °C and 3.0–5.7 GPa: new experimental data for garnet, clinopyroxene, and rutile, and implications for mantle metasomatism. *Geochim. Cosmochim. Acta* 62, 1781–1801.
- Stalder, R., Ulmer, P., Thompson, A.B., Günther, D., 2000. Experimental approach to constrain second critical end points in fluid/silicate systems: near-solidus fluids and melts in the system albite–H₂O. *Am. Mineral.* 85, 68–77.
- Tropper, P., Manning, C.E., 2005. Very low solubility of rutile in H₂O at high pressure and temperature, and its implications for Ti mobility in subduction zones. *Am. Mineral.* 90, 502–505.
- Wagner, W., Pruss, A., 2002. The IAPWS formulation 1995 for the thermodynamic properties of ordinary water substance for general and scientific use. *J. Phys. Chem. Ref. Data* 31, 387–535.
- Wilke, M., Schmidt, C., Farges, F., Malavergne, V., Gautron, L., Simionovici, A., Hahn, M., Petit, P.-E., 2006. Structural environment of iron in hydrous aluminosilicate glass and melt – evidence from X-ray absorption spectroscopy. *Chem. Geol.* 229, 144–161.
- Wirth, R., 2004. Focused Ion Beam (FIB): a novel technology for advanced application of micro- and nanoanalysis in geosciences and applied mineralogy. *Eur. J. Mineral.* 16, 863–877.